

Reanalysis of the RXTE observations of the black-hole candidate XTE J1650–500 in the 2001/2002 outburst *

Li-Hong Yan^{1,2,3} and Jian-Cheng Wang^{1,2}

¹ National Astronomical Observatories / Yunnan Observatory, Chinese Academy of Sciences, Kunming 650011, China; yanlh@ynao.ac.cn; jcwang@ynao.ac.cn

² Key Laboratory for the Structure and Evolution of Celestial Objects, Chinese Academy of Sciences, Kunming 650011, China

³ Graduate University of Chinese Academy of Sciences, Beijing 100049, China

Received 2011 April 16; accepted 2011 September 27

Abstract We present the results of the spectral fits made to 59 Rossi X-ray Timing Explorer (RXTE) observations of the Galactic X-Ray Black-Hole Candidate XTE J1650–500 covering the first 30d of its 2001/2002 outburst when the source was in a transition from the hard state to the soft state. The photon spectra can be well fitted with a phenomenological model of a power-law/cutoff power-law and a physical model of bulk-motion Comptonization. The spectral properties smoothly evolve away from the hard state and then stay in the soft state. The fitting results of the physical model reveal the peak of the burst had a flux of 2.90×10^{-8} erg cm⁻² s⁻¹ in the 2–100 keV energy range and was observed on 2001 Sep. 9; it transitioned to the hard state. The total flux decays by a factor of ~ 3 as it evolves into the soft state. The photon index Γ increases from ~ 1.5 in the hard state and stays at ~ 2.5 in the soft state. We found that the effective area of the high-energy X-ray emission region (the Compton cloud) decreases, i.e. the area of the Compton cloud decreases by a factor of ~ 23 during the transition from the hard state to the soft state. Combining the new radio and quasi-periodic oscillation studies, the model of total flux in the 2–100 keV energy range, the jet emission and the timing analysis during the state transition, we suggest a possible geometry and evolution for the (jet+corona+disk) system, like that proposed by Kalemci et al. based on enhanced lags and peak frequency shift during the transition.

Key words: accretion, accretion disks — black hole physics — X-rays binaries: individual (XTE J1650–500) — X-rays: stars

1 INTRODUCTION

Black hole X-ray binaries (BHBs) are binary systems consisting of a black hole primary in orbit with a less evolved companion star. They are observed in outbursts which are generally believed to be caused by a sudden increase in the mass accretion rate that usually lasts for a few months (Lasota

* Supported by the National Natural Science Foundation of China.

et al. 1996; Lasota 2001; Brocksopp et al. 2004) after a quiescence period lasting months to tens of years (Chen et al. 1997; Tanaka & Shibazaki 1996).

From the onset of the outburst, the system can go through its low-hard state, intermediate state (hard intermediate state and soft intermediate state; Homan & Belloni 2005; Belloni et al. 2005, 2006), very high state, high soft state and last quiet state (Tanaka & Lewin 1995; Gierliński & Newton 2006; McClintock & Remillard 2006; the state classification of Esin et al. 1997 was based on the luminosity and spectrum shape; for other definitions refer to Homan & Belloni 2005; McClintock & Remillard 2006). The outburst shows a counter-clockwise q-like structure in the hardness-intensity diagram (HID; Chen et al. 2010). During the whole outburst, the X-ray properties show large varieties and display two main spectral states, i.e. a hard state and a soft state (McClintock & Remillard 2006). The observed energy spectrum of the hard state, whose appearance of the accretion flow is not clearly known (Maccarone & Coppi 2003), is generally dominated by a hard power law ($\Gamma \sim 1.4$ – 1.7 ; Tanaka & Shibazaki 1996) with a cut-off at ~ 100 keV (Sunyaev & Truemper 1979; Grove et al. 1998) and has a faint thermal component.

Hard state spectra are generally well fitted by thermal Comptonization which show νF_ν spectrum peaks at ~ 100 keV, i.e. multiple Compton upscattering of soft photons by a Maxwellian distribution of electrons (see Sunyaev & Titarchuk 1980) in a hot ($kT_e \sim 50$ – 100 keV) plasma of Thomson optical depth τ_T of the order unity (Shapiro et al. 1976; Gierliński et al. 1997; Zdziarski et al. 1996; Zdziarski 2000; Frontera et al. 2001a,b; Wardziński et al. 2002; Zdziarski et al. 2002, 2003). By contrast, the spectrum of the soft state, which is believed to be the signature of a geometrically thin optically thick accretion disk (Shakura & Sunyaev 1973), is generally dominated by a thermal component, and usually presents a weak steep power-law component ($\Gamma \sim 2.3$ – 3.5) extending at least to MeV energies, without any hint of a high-energy cut-off (Grove et al. 1998; McConnell et al. 2000, 2002; Zdziarski & Gierliński 2004). The soft state spectrum is generally fitted well by a multi-disk black body (DISKBB) (Mitsuda et al. 1984; Makishima et al. 1986), which peaks at a few keV. The soft power law (compared to the low hard state (LHS)) is generally interpreted as inverse Compton upscattering of soft photons by a nonthermal (Poutanen & Coppi 1998; Gierliński et al. 1999; Coppi 1999; Zdziarski et al. 2001; Zdziarski & Gierliński 2004) or hybrid thermal/non-thermal distribution of electrons in a hot relativistic plasma or the so-called corona (Zdziarski et al. 2001; Ibragimov et al. 2005; Cadolle Bel et al. 2006; Malzac et al. 2006; Malzac & Belmont 2009).

The different spectral states of Galactic X-Ray Black-Hole Candidates (GBHCs) are usually understood in terms of changes in the geometry of the accretion flow. According to a popular scenario (see e.g., Done et al. 2007), in the soft state a geometrically thin accretion disk extends down to the last stable orbit and is responsible for the dominant thermal emission (Shakura & Sunyaev 1973; Pringle 1981). The disk is the source of soft seed photons for Comptonization in small active coronal regions located above and below it. The magnetic field lines rise above the accretion disk through magnetic buoyancy, transporting a significant fraction of the accretion power into the corona where it is then dissipated through magnetic reconnection (Galeev et al. 1979). This leads to particle acceleration in the corona. A population of high-energy electrons is formed and then cools down by upscattering the soft photons emitted by the disk. This produces the high-energy non-thermal emission (see e.g., Gierliński et al. 1999; Zdziarski et al. 2002). However, for the hard state, a large number of black hole binaries have been successfully modelled by a thermal Comptonization model (Dove et al. 1997; Poutanen & Svensson 1996), but the accretion geometry, the emission mechanisms, and the connection between the accreting material and the compact jet outflow present in at least some black hole candidates (BHCs) (Fender 2001) are all currently active areas of debate.

Until now, four main configurations exist for this state. First, the standard geometrically thin disk does not extend to the last stable orbit. The weakness of the thermal features instead suggests that it is truncated at distances ranging from a few tens to a few thousand gravitational radii from the black hole (typically 1000–10 000 km). In its inner parts, the accretion flow takes the form of

a hot geometrically thick, optically thin disk or the so called advection dominated accretion flow (ADAF; Ichimaru 1977; Esin et al. 1997; Poutanen et al. 1997; for modifications also see Blandford & Begelman 1999; Igumenshchev & Abramowicz 2000; Czerny et al. 2000). The relatively inefficient ADAF channels matter to the compact object and to any jets (McClintock & Remillard 2006); this region has low density and is responsible for the high-energy emission. Several models which were developed based on this model are Adiabatic Inflow-Outflow Solution (ADIOS; Blandford & Begelman 1999), Convection-Dominated Accretion Flow (CDAF; Igumenshchev & Abramowicz 1999; Stone et al. 1999; Narayan et al. 2000; Quataert & Gruzinov 2000), Luminous Hot Accretion Disk Flow (LHAF; Yuan 2001; Yuan & Zdziarski 2004) and Magnetic Dominate Accretion Flow (MDAF; Meier 2005; Fragile & Meier 2009). One contender model is the accretion disk corona (ADC; e.g., Malzac 2007) whose mechanism is subtly different.

A hot corona of energetic particles may come from above and below an accretion disk, and most of the accretion power is carried by strong magnetic fields. When the fields in the corona are strong, the emission from the corona is also strong, and a higher proportion of in-falling material is channelled into the jets (Merloni & Fabian 2002). Although both of these possibilities describe physical processes that may occur in BHBs, neither provides a complete picture of accreting BHBs because radio observations in the hard state indicate the presence of a powerful compact jet (Fender 2001). Hence, the second competing configuration is the jet which interprets the high energy emission as synchrotron and/or synchrotron self-Compton (SSC) radiation from the base of a jet where low energy photons come from the disk or ADAF (Georganopoulos et al. 2002; Markoff et al. 2003; Markoff & Nowak 2004; Markoff et al. 2005; Nowak et al. 2005; Ferreira et al. 2006; Gallo et al. 2007; Migliari et al. 2007; Tomsick et al. 2008; Maitra et al. 2009).

Considering that X-Rays could come from the base of the jet, and until now there is no evidence for relativistic beaming in either the low state or the quiescent state BHBs, Narayan (2005) claimed that the base of the jet is probably right inside the ADAF. So the problem of finding the location of the X-Ray emission, whether from the ADAF or from the jet, becomes a matter of semantics of whether this gas should be called the jet or the ADAF.

The last alternative accretion flow configuration is the bulk-motion converging sub-Keplerian flow within $50R_g$ of the black hole (Titarchuk & Shrader 2002; Turolla et al. 2002), where hard X-Ray radiation comes from the inverse Compton scattering of high energy infalling electrons on the soft photons and is called the bulk-motion Comptonization model (BMC; Colpi 1988).

In general, it may be assumed that these processes, with their different physical mechanisms, occur in systems simultaneously or episodically (Titarchuk & Seifina 2009).

XTE J1650–500 was first detected by the All-Sky Monitor (ASM, Levine et al. 1996) on board the RXTE in 2001 September (Remillard 2001) and subsequently reached a peak X-ray intensity of 0.5Crab. Subsequent observations established that XTE J1650–500 is a strong black hole candidate (BHC) based on its X-ray spectrum and variability in the X-ray light curve (Markwardt et al. 2001; Revnivtsev & Sunyaev 2001; Wijnands et al. 2001; Homan et al. 2003; Kalemci et al. 2003; Rossi et al. 2004). Orosz et al. (2004) found the period of the binary system to be 7.63 ± 0.02 hr, and the mass function (lower limit of black hole mass) to be $2.7 \pm 0.6 M_\odot$ based on optical observations. The inclination of the system is not well known, but recent studies of the companion star indicate that its minimum value is $50 \pm 3^\circ$ (Orosz et al. 2004). The optical and radio counterparts were identified by Castro-Tirado et al. (2001) and Groot et al. (2001; see also Corbel et al. 2004), respectively. The mean source position is R.A. = $16^{\text{h}}50^{\text{m}}00^{\text{s}}.98$, Dec = $-49^\circ57'43''$ (equinox J2000) with an uncertainty of $0.6''$ (Tomsick et al. 2004). This position is consistent with the radio (Groot et al. 2001) and optical (Castro-Tirado et al. 2001) positions. Combining the studies of the variability properties of this source (Kalemci et al. 2003; Homan et al. 2003; Montanari et al. 2009), previous researchers have shown that the source underwent dramatic changes in its X-ray spectral and timing properties during the 2001 X-ray outburst. Generally, the changes were not unusual for BHC X-ray transients. The source

started off in a hard state, with a hard energy spectrum and a high level of timing noise, made a transition to a soft spectral state, and then made a transition back to the hard state (Kalemci et al. 2003; Homan et al. 2003; Rossi et al. 2004, 2005; Montanari et al. 2009).

In this paper, we concentrate on 59 RXTE ToO observations covering the first 30d obtained between 2001 Sep. 6 and 2001 Oct. 5 when the source was in a transition from the hard state to the soft state. In Section 2 we describe the data reduction. Spectral fitting results, analysis of the source evolution and the accretion configurations are presented in Section 3. Section 4 gives the discussion of the fitting results.

2 DATA REDUCTION

2.1 Satellite Overview

On board the RXTE satellite there are three detectors. The ASM (Levine et al. 1996; Rothschild et al. 1998; Bradt et al. 2001; Bradt & Remillard 2001) is used to track the long-term behavior of sources in the 2–13 keV energy band. Another two scientific detectors, the Proportional Counter Array (PCA; Zhang et al. 1993; Giles 1994; Strohmayer 1994; Jahoda et al. 1996, 2006, 2008) and the High Energy X-Ray Timing Experiment (HEXTE; Hink et al. 1992; Wayne et al. 1995; Gruber et al. 1996; Rothschild et al. 1998), are two co-aligned spectrometers with narrow fields of view. They provide broad energy coverage from ~ 2 to ~ 250 keV. The PCA consists of five non-imaging Xe multiwire proportional counter units (PCUs) which cover the range 2–60 keV and have a time resolution of $\sim 1 \mu\text{s}$ (2^{-20} s). The PCA has a $1^\circ \times 1^\circ$ field of view and provides a total collecting area of $\sim 6500 \text{ cm}^2$. The HEXTE is comprised of two clusters, each with four scintillation detectors sensitive to photons in the range 15–250 keV, collimated to view a common 1° field, and these eight detectors provide a total collecting area of $\sim 1600 \text{ cm}^2$ (Gruber et al. 1996).

2.2 Data Reduction

The RXTE ToO datasets (PCA and HEXTE) on XTE J1650–500 were reduced using the HEASOFT software package version 6.8, following the standard steps described in the RXTE cookbook and REX script introduction.

For PCA data, we defined the “basic” good time intervals (GTIs) as the times during which the offset pointing was less than 0.02° from the source and the elevation above the Earth’s limb was higher than 10° . This resulted in about ~ 130 ks of good times. The spectrum was extracted from the Standard-2 mode data with a time resolution of 16 s and 129 energy channels between 2 and 60 keV with each spectrum being sampled every 16 s. All three layers of the PCU2, which is the only operational unit across all observations and is the best calibrated detector out of the five PCUs, were used to extract the PCA spectrum. The background spectra are made with the FTOOLS pcabackest version 3.8, with the latest calibration files available for the bright source. Instrument response files were obtained with the tool pcrarsp version 11.7. An additional 0.6% in systematic errors were added to all channels because of calibration uncertainties in the PCA response.

For HEXTE data, because detector-2 of HEXTE cluster-B has lost its spectral capability, the energy spectra in 15–250 keV are only derived from the cluster-A archive mode data, with a 16 s time resolution and 64 energy channels between 15 and 250 keV. The “on” and the “off” source pointings were separated before extraction of source plus background and background spectra, which were further corrected for dead time. Spectral responses were available on the HEASARC (High Energy Astrophysics Science Archive Research Center; <http://heasarc.gsfc.nasa.gov/>) web page because our extracted data had the same time resolution of 16 s and same binning pattern of 64 channel bins.

3 SPECTRAL ANALYSIS AND RESULTS: MODELING THE 3–150 keV SPECTRUM OF XTE J1650–500

3.1 Choice of Spectral Models

For fits to the combined data from PCA and HEXTE, in view of the detection sensitivity of the instruments at low energy and the signal to noise ratio at high energy, we considered the data from the PCA in the energy range 3–25 keV and HEXTE data in 18–150 keV. We performed simultaneous fits in XSPEC V12.5.1 (Arnaud 1996) which is an astrophysical spectral modelling package. The fit statistic and minimization technique in use are Chi-squared minimum and Levenberg-Marquardt, respectively. In order to account for the uncertainties in the relative calibration of the PCA and HEXTE instruments, the normalization factor accounted by the CONSTANT component in XSPEC for PCA data is always set to one and that of HEXTE data allowed to vary for simultaneous fits. According to Remillard & McClintock (2006), each of the spectral continuum models we present below includes the effect of interstellar absorption in the direction of XTE J1650–500, using the PHABS component in XSPEC with cross-sections from Balucińska-Church & McCammon (1998) and abundances from Anders & Grevesse (1989). The total column density was fixed to be $5.3 \times 10^{22} \text{ cm}^{-2}$ (Miller et al. 2002; Miniutti et al. 2004).

A major issue with describing a GBHB X-ray spectrum is the choice of models to be employed. Generally, the energy spectra of GBHBs are described jointly with black-body and power-law components (Remillard & McClintock 2006). Usually, the soft X-rays are thought to be produced in the accretion disk and modeled as disk black body emission (DISKBB; Mitsuda et al. 1984; Makishima et al. 1986; Kubota & Makishima 2004; Kubota et al. 2005). However, concerning hard X-rays, many more or less physically motivated models are available (e.g., BMC: Blandford & Payne 1981; Colpi 1988; compBB: Nishimura et al. 1986; compLS: Lamb & Sanford 1979; compPS: Poutanen & Svensson 1996 and references; Jones 1968; compST: Sunyaev & Titarchuk 1980; compTT: Hua & Titarchuk 1995; Titarchuk & Lyubarskij 1995; EQPAIR: Coppi 1992, 1999). Here, we used several models consisting of phenomenological and physical models to describe the spectral shapes of XTE J1650–500 and our approach is twofold: on the one hand, we try to fit all photon spectra with two simple phenomenological models, a power-law/cut-off power-law model (PL/CUTOFFPL) and a broken power-law model (BKNPL), in order to directly compare them with previous results. On the other hand, we study the source in the framework of physical models in an attempt to find a self-consistent scenario that can help us to understand the physics of the observed spectral evolution.

3.2 Empirical Model: PL/CUTOFFPL and BKNPL

For hard state observations, we use the same model as Rossi et al. (2005) but replace the LAOR component with a GAUSSIAN component. The model in the XSPEC terminology is CONSTANT*PHABS*SMEDGE(DISKBB+GAUSSIAN+CUTOFFPL) (hereafter MODEL 1). The cutoff power-law (CUTOFFPL is a power-law times an exponential factor) is merely an empirical approximation to the spectra expected from unsaturated Comptonization processes. A multi-color black-body disk component (DISKBB; Mitsuda et al. 1984; Makishima et al. 1986) is a simple non-relativistic approximation or non-radiative transfer to the X-ray spectrum integrated over a standard accretion disk, and it does not specify a zero-torque condition at the inner boundary (Zimmerman et al. 2005). Because we use the same low energy threshold of the PCA, we constrain the inner disk temperature to values between 0.3–0.65 keV as in Rossi et al. (2005). Taking into consideration the spectral resolution of RXTE, which is ~ 1 keV at 6 keV, and the line results given by XMM-Newton (Miller et al. 2002) and BeppoSAX (Miniutti et al. 2004; Montanari et al. 2009), we fix the line energy to 5.3 keV and the line width to 2 keV (setting these two parameters free only slightly affects the fitting results), and the E_{edge} to 7.1 keV and width to 10 keV (setting these two parameters

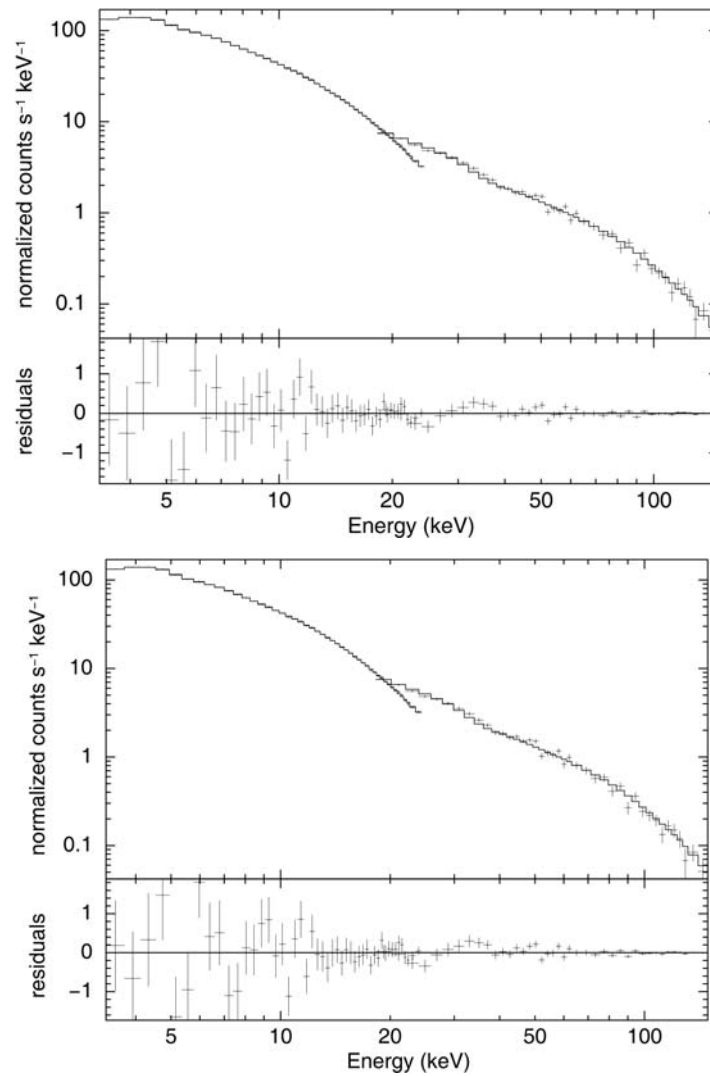


Fig. 1 *Top*: the top panel is the combined PCA/HEXTE spectrum of XTE J1650–500 for a typical observation (ObsID 60113–01–01–00) with the best-fit model being: `CONSTANT*PHABS*SMEDGE(DISKBB+GAUSSIAN+CUTOFFPL)`, and the bottom panel is the residuals of the fitting, with $\chi^2 = 1.27$ for 78 d.o.f.; *Bottom*: the top panel is the fitting spectrum with the best-fit model: `CONSTANT*PHABS*SMEDGE*HIGHECUT*BMC`, and the bottom panel is the residuals of the fitting, with $\chi^2 = 1.31$ for 82 d.o.f.

free, we get fitting values around these two values). The fitting spectrum and the residual of ObsID 60113–01–01–00 is shown in Figure 1 (Top). For such large datasets, the CPU time needed to perform spectral fitting can be considerable and therefore the choice of starting parameters for spectral modelling and how the spectral fits are performed is of some practical importance. We note that the most obvious strategy of spectral modelling, namely using the best fit values of nearby observations, can severely bias the correlations found between different spectral parameters since this strategy can

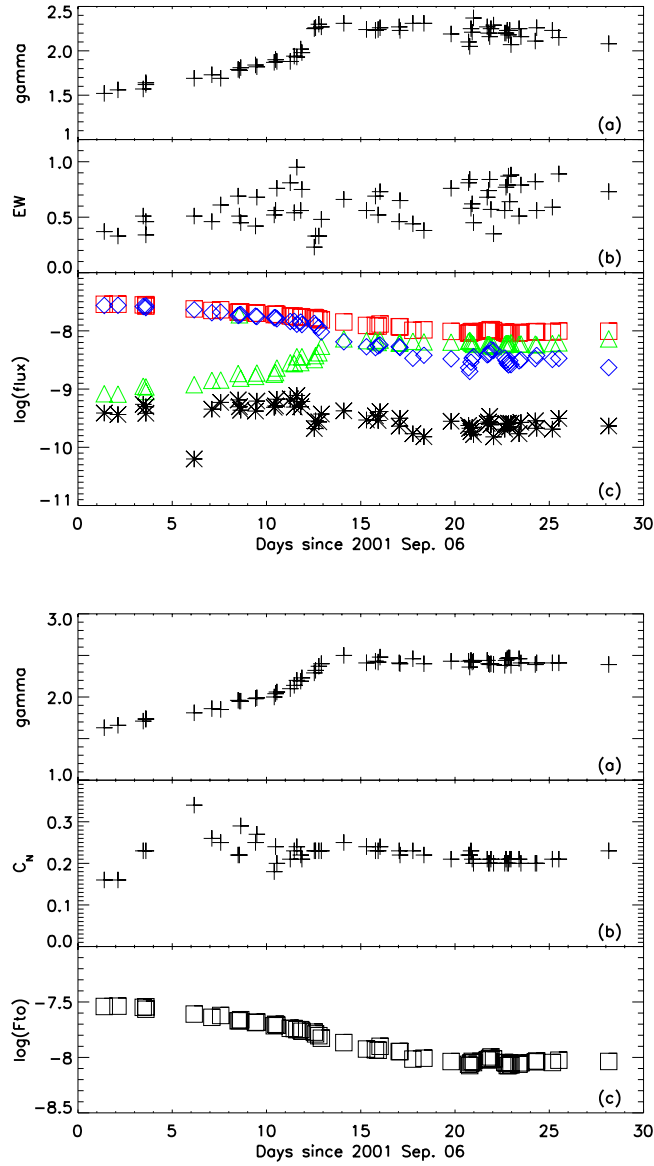


Fig. 2 *Top:* Time evolution of (a) photon index Γ , (b) EW in keV, and (c) unabsorbed flux of the total emission (*red squares*), power-law emission (*blue diamonds*), blackbody emission (*green triangles*) and the Fe-line emission (*black crosses*) in 2–100 keV in $\text{erg cm}^{-2} \text{s}^{-1}$ of MODEL 1 (*color online*). *Bottom:* Time evolution of (a) photon index Γ which is the energy spectral index $\alpha+1$, (b) the normalization of the BB component C_N , (c) the unabsorbed flux of the total emission in 2–100 keV in $\text{erg cm}^{-2} \text{s}^{-1}$ of MODEL 2.

force larger numbers of data points into local χ^2 -minima. This bias is less of an issue when always using the same starting parameters, which is the approach adopted for all of the fits described below, even though this approach requires a larger amount of CPU time. The same model cannot be used to describe the soft state observations well enough. The fitting residuals leave a noticeable discrepancy, a prominent data excess above ~ 100 keV which is due to no high-energy cutoff, and the fitting E_{cut} exceeds 150 keV that we consider here. Thus we substitute the POWERLAW component which is also a purely phenomenological approximation, which could be from a compact jet, a corona, or reprocessed emission, for CUTOFFPL. Thus far, this model can reasonably fit all datasets. Table 1 gives the best fitting parameters with all the quoted uncertainties on the parameters corresponding to 90% confidence intervals (i.e. $\Delta\chi^2 = 2.71$) for each parameter. These results we obtained are similar to the values that Rossi et al. (2004; also see Rossi et al. 2005) found. The evolution of the parameters is presented in Figure 2 (Top).

For hard state spectra, an alternative model component BKNPOWER, replacing the CUTOFFPL component in the above model, can also result in a reasonable fit to the combined data. However, we do not need a smeared edge component here, so the fitting model becomes CONSTANT*PHABS(DISKBB+GAUSSIAN+BKNPOWER) which is similar to that of Zhang et al. (2007). The break energy E_{break} decreases from ~ 40 to ~ 27 keV, while the photon index of Γ_1 before the break energy increases from ~ 1.58 to ~ 2 and that of Γ_2 after the break energy increases from ~ 2.2 to ~ 2.6 . This evolution trend is similar that of Zhang et al. (2007), but opposite to that of Wilms et al. (2006), who physically interpreted Γ_2 to be less than Γ_1 as the hardening of the underlying continuum caused by Compton reflection off cold or mildly ionized material. Γ_1 in our fitting is similar to the photon index Γ of the CUTOFFPL component in MODEL 1 and can be classified as hard state with a simplified version of the classification of Remillard (2005). From the χ^2/ν values, only in 6 out of the 22 observations are the BKNPOWER fits better than those of the CUTOFFPL fits.

3.3 Physical Comptonization Model: COMPTT and BMC

To find an interpretation of the empirically derived spectral shape in terms of Comptonization, we used the thermal Comptonization model compTT (Titarchuk 1994; see also Titarchuk & Lyubarskij 1995; Titarchuk & Hua 1995), which describes the Comptonization of the soft seed photons from the disk by the hot plasma, as historically it has met with good success in describing black hole spectra. Assuming a spherical geometry (for hard state; disk geometry for soft state), the parameters of the continuum are the electron optical depth, τ_e , and the electron temperature kT_e . So we replace the CUTOFFPL component with the compTT component in MODEL 1 and set the temperature of the seed photons for Comptonization equal to the DISKBB temperature kT_{in} , indicating that the disk is the source of the seed photons. This model, CONSTANT*PHABS*SMEDGE(DISKBB+GAUSSIAN+COMPTT), gives a good fit to all datasets in a χ^2 sense ($\chi^2/\nu \sim 1$). Although the thermal Comptonization model can properly fit all observed spectra, it would give physically unreasonable values of the best-fit parameters for soft spectra. Notably, we found that the optical depth τ of the Compton cloud inferred from this model significantly decreases from ~ 4.5 to ~ 1.5 toward the soft state, confirming the statement of Wilms et al. (2006). It is very difficult (in the framework of any reasonable physical model) to justify this tendency of τ to decrease when the mass accretion rate increases during the hard-to-soft state transition (e.g., Shaposhnikov & Titarchuk 2006). However, the photon index Γ inferred using the best-fit parameters τ and kT_e is a physical characteristic of the Comptonization process. In fact, the photon index Γ is the reciprocal of the Comptonization parameter Y (Bradshaw et al. 2007) and is independent of any type or model of Comptonization (thermal or bulk). Notably, this approach is only approximately justified, since the seed photon distribution assumed by compTT is a Wien distribu-

Table 1 Best-fit Parameters of the Spectral Analysis of the PCA and HEXTE Observation of XTE J1650–500 in the Energy Range 3–150 keV during the 2001/2002 Outburst with the Model CONSTANT*PHABS*SMEDGE (DISKBB+GAUSSIAN+CUTOFF/PL)

ObsID	T_{exp} (ks)	Γ	E_{cut} (keV)	EW (keV)	F_{to} (erg cm ⁻² s ⁻¹)	F_{bb}	F_{pl}	$\chi^2/\text{d.o.f.}$ $\Delta\chi^2 = 2.71$
60113-01-01-00	0.480	1.51 ± 0.06	107 ± 18	0.34	2.61 × 10 ⁻⁸	5.92 × 10 ⁻¹⁰	2.52 × 10 ⁻⁸	1.27
60113-01-03-00	3.312	1.52 ± 0.04	91 ⁺⁷ ₋₄	0.37	2.86 × 10 ⁻⁸	8.32 × 10 ⁻¹⁰	2.73 × 10 ⁻⁸	1.24
60113-01-04-00	3.312	1.56 ± 0.04	93 ± 7	0.33	2.87 × 10 ⁻⁸	8.20 × 10 ⁻¹⁰	2.75 × 10 ⁻⁸	0.91
60113-01-05-00	2.176	1.57 ± 0.04	89 ⁺⁸ ₋₉	0.51	2.79 × 10 ⁻⁸	1.12 × 10 ⁻⁹	2.62 × 10 ⁻⁸	0.72
60113-01-05-01	1.472	1.64 ± 0.03	109 ⁺¹³ ₋₉	0.34	2.82 × 10 ⁻⁸	9.08 × 10 ⁻¹⁰	2.69 × 10 ⁻⁸	1.05
60113-01-05-01	1.472	1.62 ± 0.05	95 ⁺¹⁰ ₋₇	0.46	2.66 × 10 ⁻⁸	1.09 × 10 ⁻⁹	2.51 × 10 ⁻⁸	1.05
60113-01-07-00	2.960	1.69 ± 0.05	98 ⁺¹¹ ₋₉	0.51	2.38 × 10 ⁻⁸	1.19 × 10 ⁻⁹	2.30 × 10 ⁻⁸	0.92
60113-01-08-00	2.048	1.73 ± 0.08	87 ⁺¹³ ₋₅	0.46	2.24 × 10 ⁻⁸	1.41 × 10 ⁻⁹	2.05 × 10 ⁻⁸	1.34
60113-01-08-01	1.584	1.69 ± 0.05	87 ⁺¹³ ₋₇	0.61	2.30 × 10 ⁻⁸	1.43 × 10 ⁻⁹	2.10 × 10 ⁻⁸	0.84
60113-01-09-00	1.872	1.79 ± 0.05	98 ⁺¹⁶ ₋₁₀	0.69	2.09 × 10 ⁻⁸	1.85 × 10 ⁻⁹	1.84 × 10 ⁻⁸	0.98
60113-01-09-01	1.616	1.78 ± 0.07	91 ⁺¹⁷ ₋₁₁	0.51	2.10 × 10 ⁻⁸	1.89 × 10 ⁻⁸	1.89 × 10 ⁻⁸	1.24
60113-01-09-02	1.392	1.81 ± 0.09	103 ± 18	0.45	2.12 × 10 ⁻⁸	1.54 × 10 ⁻⁹	1.92 × 10 ⁻⁸	1.00
60113-01-10-00	1.984	1.84 ± 0.05	102 ⁺¹⁶ ₋₁₃	0.42	2.01 × 10 ⁻⁸	1.65 × 10 ⁻⁹	1.80 × 10 ⁻⁸	0.89
60113-01-10-01	1.888	1.82 ± 0.06	105 ⁺²² ₋₁₃	0.68	2.01 × 10 ⁻⁸	1.89 × 10 ⁻⁹	1.76 × 10 ⁻⁸	0.87
60113-01-11-00	2.176	1.87 ± 0.06	103 ⁺²⁰ ₋₁₄	0.52	1.90 × 10 ⁻⁸	1.80 × 10 ⁻⁹	1.68 × 10 ⁻⁸	0.75
60113-01-11-01	1.984	1.90 ± 0.08	123 ⁺³³ ₋₂₀	0.56	1.93 × 10 ⁻⁸	1.92 × 10 ⁻⁹	1.69 × 10 ⁻⁸	0.86
60113-01-11-02	1.696	1.88 ± 0.06	123 ⁺³⁰ ₋₂₄	0.76	1.91 × 10 ⁻⁸	2.30 × 10 ⁻⁹	1.61 × 10 ⁻⁸	0.84
60113-01-12-00	3.136	1.88 ^{+0.06} _{-0.03}	100 ⁺¹⁸ ₋₁₂	0.81	1.80 × 10 ⁻⁸	2.83 × 10 ⁻⁹	1.45 × 10 ⁻⁸	1.04
60113-01-12-01	2.000	1.94 ± 0.07	100 ⁺²⁶ ₋₁₆	0.54	1.78 × 10 ⁻⁸	2.73 × 10 ⁻⁹	1.46 × 10 ⁻⁸	1.37
60113-01-12-02	1.552	1.93 ± 0.07	102 ⁺³³ ₋₁₉	0.95	1.74 × 10 ⁻⁸	3.60 × 10 ⁻⁹	1.30 × 10 ⁻⁸	0.86
60113-01-12-03	9.760	2.02 ± 0.10	121 ⁺⁶³ ₋₃₀	0.56	1.75 × 10 ⁻⁸	2.85 × 10 ⁻⁹	1.42 × 10 ⁻⁸	0.87
60113-01-12-04	1.040	1.98 ^{+0.15} _{-0.08}	113 ⁺⁶⁷ ₋₂₀	0.75	1.70 × 10 ⁻⁸	3.60 × 10 ⁻⁹	1.28 × 10 ⁻⁸	1.03
60113-01-13-00	1.808	2.25 ± 0.04		0.23	1.69 × 10 ⁻⁸	3.21 × 10 ⁻⁹	1.35 × 10 ⁻⁸	1.08
60113-01-13-01	1.456	2.26 ± 0.05		0.33	1.65 × 10 ⁻⁸	3.76 × 10 ⁻⁹	1.24 × 10 ⁻⁸	1.14
60113-01-13-02	0.896	2.30 ^{+0.06} _{-0.08}		0.33	1.59 × 10 ⁻⁸	4.20 × 10 ⁻⁹	1.14 × 10 ⁻⁸	0.97
60113-01-14-00	3.056	2.27 ± 0.04		0.48	1.54 × 10 ⁻⁸	5.44 × 10 ⁻⁹	9.56 × 10 ⁻⁹	0.95
60113-01-15-00	3.552	2.31 ± 0.06		0.66	1.42 × 10 ⁻⁸	7.29 × 10 ⁻⁹	6.49 × 10 ⁻⁹	1.05
60113-01-16-00	2.128	2.24 ± 0.07		0.56	1.24 × 10 ⁻⁸	6.79 × 10 ⁻⁹	5.33 × 10 ⁻⁹	1.16
60113-01-16-01	1.136	2.23 ± 0.10		0.69	1.22 × 10 ⁻⁸	6.74 × 10 ⁻⁹	5.15 × 10 ⁻⁹	0.79
60113-01-16-02	0.656	2.24 ^{+0.09} _{-0.16}		0.52	1.21 × 10 ⁻⁸	6.31 × 10 ⁻⁹	5.53 × 10 ⁻⁹	0.85
60113-01-17-00	5.408	2.26 ± 0.06		0.73	1.31 × 10 ⁻⁸	6.95 × 10 ⁻⁹	5.72 × 10 ⁻⁹	0.91
60113-01-18-00	1.776	2.27 ^{+0.04} _{-0.15}		0.46	1.18 × 10 ⁻⁸	6.19 × 10 ⁻⁹	5.37 × 10 ⁻⁹	0.78
60113-01-18-01	3.760	2.23 ± 0.06		0.65	1.17 × 10 ⁻⁸	6.25 × 10 ⁻⁹	5.18 × 10 ⁻⁹	1.14
60113-01-18-02	0.864	2.31 ± 0.14		0.44	1.02 × 10 ⁻⁸	6.63 × 10 ⁻⁹	3.38 × 10 ⁻⁹	0.99
60113-01-19-00	2.064	2.31 ^{+0.08} _{-0.16}		0.38	1.04 × 10 ⁻⁸	6.47 × 10 ⁻⁹	3.81 × 10 ⁻⁹	0.74
60113-01-19-01	0.432	2.19 ^{+0.15} _{-0.25}		0.76	9.78 × 10 ⁻⁹	6.40 × 10 ⁻⁹	3.30 × 10 ⁻⁹	0.66
60113-01-19-02	0.496	2.10 ^{+0.22} _{-0.16}		0.81	9.18 × 10 ⁻⁹	6.62 × 10 ⁻⁹	2.32 × 10 ⁻⁹	0.73
60113-01-19-03	0.416	2.25 ^{+0.17} _{-0.24}		0.58	9.53 × 10 ⁻⁹	6.44 × 10 ⁻⁹	2.90 × 10 ⁻⁹	0.87
60113-01-19-04	0.336	2.05 ^{+0.31} _{-0.14}		0.84	9.13 × 10 ⁻⁹	6.90 × 10 ⁻⁹	2.01 × 10 ⁻⁹	1.01
60113-01-19-05	0.464	2.21 ^{+0.16} _{-0.19}		0.62	9.74 × 10 ⁻⁹	6.14 × 10 ⁻⁹	3.39 × 10 ⁻⁹	0.87
60113-01-19-06	0.448	2.37 ± 0.16		0.45	9.63 × 10 ⁻⁹	5.85 × 10 ⁻⁹	3.61 × 10 ⁻⁹	0.80
60113-01-20-00	0.480	2.27 ± 0.18		0.68	9.97 × 10 ⁻⁹	5.85 × 10 ⁻⁹	3.87 × 10 ⁻⁹	1.11

Table 1 – *Continued.*

ObsID	T_{exp} (ks)	Γ	E_{cut} (keV)	EW (keV)	F_{to} (erg cm $^{-2}$ s $^{-1}$)	F_{bb}	F_{pl}	$\chi^2/\text{d.o.f.}$ $\Delta\chi^2 = 2.71$
60113-01-20-01	0.448	2.20 \pm 0.17		0.74	1.00 \times 10 $^{-8}$	5.83 \times 10 $^{-9}$	3.97 \times 10 $^{-9}$	0.78
60113-01-20-02	0.416	2.16 \pm 0.14		0.84	1.03 \times 10 $^{-8}$	5.78 \times 10 $^{-9}$	4.17 \times 10 $^{-9}$	1.02
60113-01-20-03	0.432	2.25 \pm 0.13		0.57	1.05 \times 10 $^{-8}$	5.55 \times 10 $^{-9}$	4.74 \times 10 $^{-9}$	0.79
60113-01-20-04	0.480	2.29 $^{+0.16}_{-0.20}$		0.35	1.01 \times 10 $^{-8}$	5.37 \times 10 $^{-9}$	4.61 \times 10 $^{-9}$	0.77
60113-01-21-00	0.352	2.20 $^{+0.22}_{-0.01}$		0.56	9.40 \times 10 $^{-9}$	5.76 \times 10 $^{-9}$	3.43 \times 10 $^{-9}$	0.83
60113-01-21-01	0.432	2.20 $^{+0.18}_{-0.20}$		0.77	9.41 \times 10 $^{-9}$	6.06 \times 10 $^{-9}$	3.09 \times 10 $^{-9}$	0.75
60113-01-21-02	0.400	2.23 $^{+0.20}_{-0.17}$		0.79	9.11 \times 10 $^{-9}$	6.00 \times 10 $^{-9}$	2.78 \times 10 $^{-9}$	1.05
60113-01-21-03	0.400	2.18 $^{+0.16}_{-0.23}$		0.87	8.96 \times 10 $^{-9}$	6.11 \times 10 $^{-9}$	2.60 \times 10 $^{-9}$	1.12
60113-01-21-04	0.432	2.23 $^{+0.17}_{-0.23}$		0.64	9.24 \times 10 $^{-9}$	5.94 \times 10 $^{-9}$	3.08 \times 10 $^{-9}$	0.94
60113-01-21-05	0.400	2.07 \pm 0.19		0.88	9.14 \times 10 $^{-9}$	6.25 \times 10 $^{-9}$	2.63 \times 10 $^{-9}$	1.05
60113-01-22-00	2.304	2.25 $^{+0.07}_{-0.14}$		0.51	9.13 \times 10 $^{-9}$	5.91 \times 10 $^{-9}$	3.05 \times 10 $^{-9}$	0.70
60113-01-22-01	3.280	2.16 \pm 0.08		0.79	9.42 \times 10 $^{-9}$	5.97 \times 10 $^{-9}$	3.18 \times 10 $^{-9}$	0.89
60113-01-23-00	5.664	2.26 \pm 0.07		0.56	9.73 \times 10 $^{-9}$	5.74 \times 10 $^{-9}$	3.78 \times 10 $^{-9}$	0.83
60113-01-23-01	2.048	2.11 \pm 0.11		0.82	9.55 \times 10 $^{-9}$	5.94 \times 10 $^{-9}$	3.33 \times 10 $^{-9}$	0.73
60113-01-24-00	6.928	2.23 \pm 0.07		0.59	9.50 \times 10 $^{-9}$	6.06 \times 10 $^{-9}$	3.23 \times 10 $^{-9}$	0.96
60113-01-24-01	1.056	2.15 $^{+0.20}_{-0.07}$		0.89	9.92 \times 10 $^{-9}$	6.23 \times 10 $^{-9}$	3.37 \times 10 $^{-9}$	0.80
60113-01-25-00	2.624	2.08 \pm 0.12		0.73	9.85 \times 10 $^{-9}$	7.28 \times 10 $^{-9}$	2.34 \times 10 $^{-9}$	0.87

Columns are Observation ID, PCA exposure time in ks, photon index Γ , high energy cutoff E_{cut} in keV in the hard state, equivalent width of the line emission EW in keV, the unabsorbed flux of total emission, blackbody emission and the power-law emission in 2–100 keV in erg cm $^{-2}$ s $^{-1}$ and reduced chi-squared values, respectively. All the quoted uncertainties of the parameters correspond to 90% confidence intervals for each parameter.

tion and not a proper disk spectrum. So we focus on the fitting results in the hard state, and only in 4 and 6 out of the 22 observations are the χ^2/ν of the compTT fits better than those of the CUTOFFPL fits and BKNPOWER fits, respectively. In spite of the caveats of the large errors, the average value of the temperature of the seed photons from the accretion disk derived from this model, \sim 0.46 keV on average, matches the temperature of the accretion disk derived from the two fits mentioned above (although it is slightly higher).

We have also fitted the observations with the alternative Comptonization model, BMC (Blandford & Payne 1981; Colpi 1988; Titarchuk et al. 1997), which correctly takes into account the relativistic effects in the Compton-scattering kinematics, allowing us to use a DISKBB model as the seed photon source, and has a built-in function to allow a part of the initial Compton-produced photons to get into cold matter and be reflected. It also takes into account the dynamical Comptonization (converging inflow, expected in the vicinity of the central object) along with the thermal Comptonization, to fit the observed spectra. This model can be used if the photon energy is less than the mean electron energy of the Compton cloud E_{av} . The choice of this model is provided by the robust nature of the BMC model for different spectral states (hard state: Laurent & Titarchuk 1999; Shrader & Titarchuk 1999; soft state: Turolla et al. 2002) and the independence of the specific type of Comptonization scenario involved. Firstly, we use an absorbed BMC model to fit the observed spectra (take ObsID 60113-01-01-00 for example). The apparent sinusoidal pattern of the residuals to the model is a clear sign of the bad fit quality. There is an excess between 4 and 6 keV and a prominent negative residual between 6 and 9 keV (with $\chi^2/\nu=4.92$ for 84 d.o.f, NHP= 6.55×10^{-45}). Thus, secondly, we add a smeared edge component SMEDGE to model the absorption feature (with $\chi^2/\nu=3.99$ for 83 d.o.f, NHP= 2.16×10^{-31}). Fortunately, the SMEDGE component also smoothed out the emission feature and drastically improved the fitting. However, for the only remaining high-energy cutoff in the spectra due to the recoil effect which is neglected

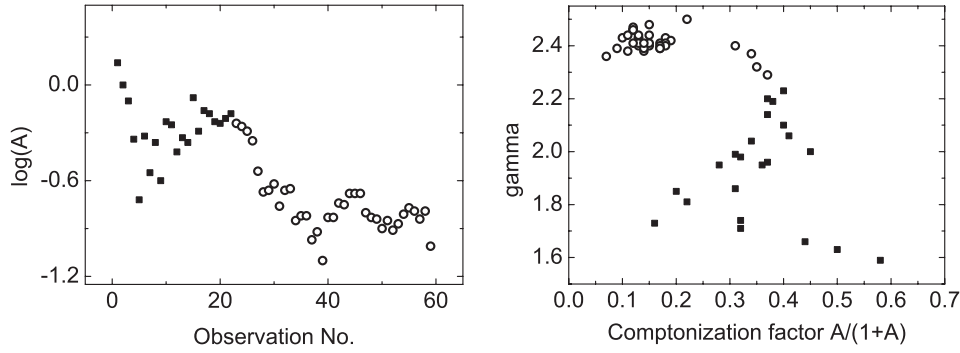


Fig. 3 *Left*: Evolution of the Compton cloud area during the spectral transition exemplified by the progressive number of time intervals. Solid boxes correspond to the hard state, and hollow circles correspond to the soft state. *Right*: Evolution of the Comptonization fraction $f = A/(1 + A)$ during the spectral transition from the hard state to the soft state. Colors are the same as the left plot.

by the BMC model at high energy, we modelled it with HIGHECUT and eventually achieved statistically acceptable fits (i.e. $\chi^2/\nu=1.31$ for 82 d.o.f, $NHP=3.03 \times 10^{-2}$). Therefore, the best fitting model is CONSTANT*PHABS*SMEDGE*HIGHECUT*BMC (hereafter MODEL 2) for hard state spectra. Figure 1 (Bottom) gives the fitting residual of the dataset ObsID 60113–01–01–00. Soft spectra do not need a HIGHECUT component. Table 2 below gives the best-fit parameters and Figure 2 (Bottom) gives their evolution with time. The total flux decays by a factor of ~ 3 , and the photon index ($\alpha + 1$) increases from ~ 1.5 to ~ 2.5 , which are all similar to MODEL 1.

One of the parameters of the BMC model is the normalization of the BB component C_N , which is directly related to the effective area A_{bb}^{eff} of the BB emission [$A_{bb}^{eff} \propto C_N/(T_{bb}^4(1 + A))$]. If we multiply this effective area with the fraction of the Comptonized component $f = A/(1 + A)$, we obtain the effective area of the high-energy X-ray emission region (the Compton cloud). Using the best-fit values for the hard state and the soft state spectra, we find that the area of the Compton cloud decreases by a factor of ~ 23 during the transition from hard-to-soft. This can be seen clearly in Figure 3. The BMC model spectrum is the sum of a BB component (which is the disk radiation directly seen by the observer) and the Comptonized fraction of a BB component in the corona. Comparing our model components to those of Montanari et al. (2009) with CONSTANT*WABS*SMEDGE*HIGHECUT(BBODY+BMC), we think that our missing BBODY component (single temperature black body model) is due to the low energy threshold at 3 keV in our spectral analysis. The low energy threshold of BeppoSAX, 0.12 keV, leads to the area of the Compton cloud decreasing less.

As can be seen from the above fitting results, we can see two physically motivated models above describing the X-ray data nearly as well in a χ^2 sense (see also Nowak et al. 2002). However, it is difficult to directly compare the spectral parameters obtained from them, as they often make different implicit assumptions in their physical setup (Nowak et al. 2002; Coppi 2004 and references therein). Comptonization models differ in their assumptions on the spectral shape of the seed photons (e.g., a Wien spectrum versus a blackbody spectrum versus an accretion disk spectrum) and they also assume different geometries for the source of the seed photons and of the Comptonizing medium (Nowak et al. 2002; Coppi 2004 and references therein). The best-fitting χ^2/ν state in 16 out of the 22 hard spectra with the COMPTT component is clearly better than the BMC component. As can be seen from Figure 4, we present observational evidence of the index saturation with

Table 2 Best-fit Parameters of Spectral Analysis of the PCA and HEXTE Observation of XTE J1650–500 in the 3–150 keV Energy Range during the 2001/2002 Outburst with the Model of CONSTANT*PHABS*SMEDGE*HIGHECUT*BMC

ObsID	kT_{bb} (keV)	α	C_N	$\log(A)$	E_{fold} (keV)	τ_{max}	$F_{\text{to}}(2 - 100 \text{ keV})$ ($\text{erg cm}^{-2} \text{ s}^{-1}$)	$\chi^2/\text{d.o.f.}$ $\Delta\chi^2 = 2.71$
60113-01-01-00	$0.34^{+0.17}_{-0.11}$	0.59 ± 0.02	0.10	0.14	131^{+19}_{-15}	1.44 ± 0.15	2.61×10^{-8}	1.31
60113-01-03-00	0.34 ± 0.10	0.63 ± 0.01	0.16	-0.00	110 ± 5	1.76 ± 0.08	2.88×10^{-8}	1.46
60113-01-04-00	$0.32^{+0.11}_{-0.08}$	0.66 ± 0.01	0.16	-0.10	112 ± 5	1.75 ± 0.08	2.90×10^{-8}	1.12
60113-01-05-00	0.30 ± 0.08	0.71 ± 0.01	0.23	-0.34	115 ± 7	1.74 ± 0.09	2.83×10^{-8}	1.10
60113-01-05-01	$0.26^{+0.09}_{-0.07}$	0.73 ± 0.01	0.45	-0.72	136 ± 12	1.67 ± 0.10	2.86×10^{-8}	1.23
60113-01-06-00	0.31 ± 0.08	0.74 ± 0.01	0.23	-0.32	118 ± 8	1.84 ± 0.09	2.72×10^{-8}	1.27
60113-01-07-00	0.29 ± 0.08	0.81 ± 0.01	0.34	-0.55	122 ± 9	1.95 ± 0.09	2.46×10^{-8}	1.19
60113-01-08-00	$0.31^{+0.05}_{-0.07}$	0.86 ± 0.01	0.26	-0.36	112 ± 10	2.08 ± 0.10	2.30×10^{-8}	1.55
60113-01-08-01	0.28 ± 0.08	0.85 ± 0.01	0.25	-0.60	122 ± 13	1.90 ± 0.11	2.39×10^{-8}	1.20
60113-01-09-00	0.34 ± 0.06	0.96 ± 0.01	0.22	-0.23	138^{+18}_{-15}	2.09 ± 0.11	2.14×10^{-8}	1.29
60113-01-09-01	0.33 ± 0.06	0.95 ± 0.01	0.22	-0.25	135^{+22}_{-17}	2.12 ± 0.11	2.15×10^{-8}	1.59
60113-01-09-02	$0.31^{+0.05}_{-0.07}$	0.95 ± 0.01	0.29	-0.42	143^{+28}_{-20}	2.01 ± 0.12	2.19×10^{-8}	1.22
60113-01-10-00	0.33 ± 0.05	0.98 ± 0.01	0.25	-0.33	146^{+20}_{-16}	2.21 ± 0.10	2.06×10^{-8}	1.24
60113-01-10-01	0.32 ± 0.06	0.99 ± 0.01	0.27	-0.36	158^{+27}_{-20}	2.08 ± 0.11	2.08×10^{-8}	1.22
60113-01-11-00	$0.38^{+0.03}_{-0.05}$	1.00 ± 0.01	0.18	-0.08	135^{+19}_{-15}	2.21 ± 0.11	1.93×10^{-8}	0.97
60113-01-11-01	$0.34^{+0.03}_{-0.06}$	1.04 ± 0.01	0.24	-0.29	175^{+38}_{-26}	2.18 ± 0.12	1.99×10^{-8}	1.14
60113-01-11-02	$0.37^{+0.03}_{-0.05}$	1.06 ± 0.01	0.20	-0.16	205^{+66}_{-40}	2.30 ± 0.12	1.95×10^{-8}	1.11
60113-01-12-00	0.39 ± 0.03	1.10 ± 0.01	0.21	-0.18	170^{+30}_{-23}	2.45 ± 0.10	1.83×10^{-8}	1.48
60113-01-12-01	0.38 ± 0.03	1.14 ± 0.02	0.23	-0.23	172^{+44}_{-31}	2.49 ± 0.12	1.82×10^{-8}	1.77
60113-01-12-02	0.39 ± 0.03	1.20 ± 0.02	0.24	-0.24	241^{+170}_{-74}	2.56 ± 0.15	1.78×10^{-8}	1.30
60113-01-12-03	0.39 ± 0.03	1.19 ± 0.03	0.22	-0.21	212^{+123}_{-60}	2.40 ± 0.16	1.78×10^{-8}	1.03
60113-01-12-04	0.42 ± 0.03	1.23 ± 0.03	0.21	-0.18	248^{+189}_{-79}	2.54 ± 0.16	1.72×10^{-8}	1.14
60113-01-13-00	0.42 ± 0.02	1.29 ± 0.01	0.23	-0.24		2.61 ± 0.11	1.69×10^{-8}	1.10
60113-01-13-01	0.44 ± 0.02	1.32 ± 0.01	0.23	-0.26		2.73 ± 0.12	1.63×10^{-8}	1.20
60113-01-13-02	0.45 ± 0.02	1.37 ± 0.02	0.23	-0.29		2.93 ± 0.15	1.57×10^{-8}	0.99
60113-01-14-00	0.49 ± 0.01	1.40 ± 0.01	0.23	-0.35		3.25 ± 0.11	1.49×10^{-8}	1.35
60113-01-15-00	0.50 ± 0.01	1.50 ± 0.01	0.25	-0.54		3.81 ± 0.13	1.36×10^{-8}	1.44
60113-01-16-00	0.50 ± 0.01	1.41 ± 0.02	0.24	-0.67		3.82 ± 0.16	1.19×10^{-8}	1.34
60113-01-16-01	0.49 ± 0.01	1.43 ± 0.02	0.23	-0.66		3.85 ± 0.20	1.17×10^{-8}	0.89
60113-01-16-02	0.50 ± 0.01	1.42 ± 0.03	0.23	-0.62		3.84 ± 0.24	1.16×10^{-8}	0.92
60113-01-17-00	0.49 ± 0.01	1.48 ± 0.01	0.24	-0.76		3.93 ± 0.12	1.26×10^{-8}	1.49
60113-01-18-00	0.49 ± 0.01	1.41 ± 0.02	0.23	-0.66		3.88 ± 0.17	1.13×10^{-8}	0.89
60113-01-18-01	0.49 ± 0.01	1.40 ± 0.01	0.22	-0.65		3.73 ± 0.13	1.13×10^{-8}	1.32
60113-01-18-02	0.49 ± 0.01	1.46 ± 0.04	0.23	-0.85		4.27 ± 0.29	9.66×10^{-9}	0.96
60113-01-19-00	0.49 ± 0.01	1.40 ± 0.02	0.22	-0.82		4.15 ± 0.19	9.84×10^{-9}	0.75
60113-01-19-01	0.49 ± 0.01	1.43 ± 0.05	0.21	-0.82		4.00 ± 0.39	9.18×10^{-9}	0.81
60113-01-19-02	0.49 ± 0.01	1.43 ± 0.06	0.22	-0.97		4.37 ± 0.42	8.67×10^{-9}	0.76
60113-01-19-03	0.48 ± 0.01	1.44 ± 0.06	0.23	-0.92		4.25 ± 0.42	8.96×10^{-9}	0.87
60113-01-19-04	0.49 ± 0.01	1.36 ± 0.08	0.22	-1.10		4.67 ± 0.57	8.44×10^{-9}	1.05
60113-01-19-05	0.48 ± 0.01	1.42 ± 0.05	0.21	-0.83		4.06 ± 0.37	9.22×10^{-9}	0.90
60113-01-19-06	0.49 ± 0.01	1.43 ± 0.05	0.20	-0.83		3.82 ± 0.39	8.99×10^{-9}	0.95
60113-01-20-00	0.48 ± 0.01	1.44 ± 0.04	0.21	-0.74		3.91 ± 0.33	9.49×10^{-9}	1.09
60113-01-20-01	0.49 ± 0.01	1.40 ± 0.04	0.20	-0.75		3.93 ± 0.34	9.60×10^{-9}	0.82
60113-01-20-02	0.49 ± 0.01	1.39 ± 0.04	0.20	-0.68		3.78 ± 0.33	9.79×10^{-9}	1.08

Table 2 – *Continued.*

ObsID	kT_{bb} (keV)	α	C_N	$\log(A)$	E_{fold} (keV)	τ_{max}	$F_{\text{to}}(2 - 100 \text{ keV})$ ($\text{erg cm}^{-2} \text{ s}^{-1}$)	$\chi^2/\text{d.o.f.}$ $\Delta\chi^2 = 2.71$
60113-01-20-03	0.48 ± 0.01	1.40 ± 0.04	0.21	-0.68		3.59 ± 0.31	1.01×10^{-8}	0.81
60113-01-20-04	0.49 ± 0.01	1.39 ± 0.04	0.20	-0.68		3.63 ± 0.31	9.70×10^{-9}	0.81
60113-01-21-00	0.49 ± 0.01	1.38 ± 0.05	0.20	-0.80		4.08 ± 0.40	9.00×10^{-9}	0.83
60113-01-21-01	0.48 ± 0.01	1.44 ± 0.05	0.21	-0.83		4.33 ± 0.39	8.91×10^{-9}	0.79
60113-01-21-02	0.49 ± 0.01	1.46 ± 0.06	0.20	-0.84		4.07 ± 0.43	8.45×10^{-9}	1.11
60113-01-21-03	0.49 ± 0.01	1.47 ± 0.06	0.20	-0.90		3.81 ± 0.45	8.44×10^{-9}	1.15
60113-01-21-04	0.48 ± 0.01	1.47 ± 0.05	0.21	-0.85		4.14 ± 0.40	8.80×10^{-9}	0.95
60113-01-21-05	0.49 ± 0.01	1.38 ± 0.06	0.21	-0.91		4.55 ± 0.44	8.55×10^{-9}	1.10
60113-01-22-00	0.48 ± 0.01	1.46 ± 0.02	0.21	-0.87		4.03 ± 0.20	8.68×10^{-9}	0.86
60113-01-22-01	0.49 ± 0.01	1.41 ± 0.02	0.20	-0.81		3.99 ± 0.16	8.93×10^{-9}	1.12
60113-01-23-00	0.49 ± 0.01	1.41 ± 0.01	0.20	-0.77		3.99 ± 0.13	9.29×10^{-9}	0.96
60113-01-23-01	0.49 ± 0.01	1.39 ± 0.02	0.20	-0.79		4.13 ± 0.19	9.13×10^{-9}	0.98
60113-01-24-00	0.49 ± 0.01	1.41 ± 0.01	0.21	-0.84		4.15 ± 0.13	9.00×10^{-9}	1.15
60113-01-24-01	0.49 ± 0.01	1.41 ± 0.03	0.21	-0.79		3.94 ± 0.24	9.44×10^{-9}	0.83
60113-01-25-00	0.50 ± 0.01	1.39 ± 0.03	0.23	-1.01		4.61 ± 0.22	9.20×10^{-9}	1.09

Columns are Observation ID, temperature of thermal photon source in keV, energy spectral index α , normalization of the BB component C_N , parameter A that is related to the weight $[A/(1+A)]$ of the Comptonization component, E-folding energy, maximum absorption optical depth, the unabsorbed flux of total emission in 2–100 keV in $\text{erg cm}^{-2} \text{ s}^{-1}$ and reduced chi-squared values, respectively. All the quoted uncertainties in the parameters correspond to 90% confidence intervals for each parameter.

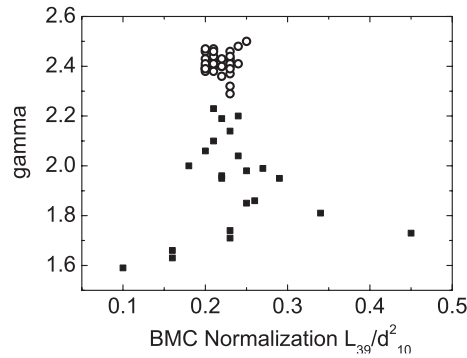


Fig. 4 Photon index evolution as a function of BMC normalization L_{39}/d_{10}^2 (which is proportional to mass accretion rate in the disk). Solid boxes correspond to the hard state, and hollow circles correspond to the soft state.

L_{39}/d_{10}^2 (and thus with mass accretion rate \dot{m}) in soft spectra with 59 RXTE ToO observational data in addition to the three BeppoSAX observations in Montanari et al. (2009). This can be considered as an observational signature of a converging flow in XTE J1650–500 (Titarchuk & Zannias 1998; Titarchuk & Fiorito 2004). Therefore, it seems likely that the thermal Comptonization and the dynamical (bulk motion) Comptonization are responsible for the spectral formation in the hard state and the soft state, respectively. The photon index, obtained using the COMPTT best-fit optical

depth τ and electron temperature kT_e and using the formula for the index related to τ and kT_e (see Titarchuk & Lyubarskij 1995), is similar to that inferred using BMC.

4 DISCUSSION

In this paper, we have reanalyzed the 59 pointed RXTE observations of the GBHC XTE J1650–500 covering the period between 2001 Sep. 6 and 2001 Oct. 5 when the source was in a transition from the hard state to the soft state and in the soft state itself. All the combined spectra of PCA and HEXTE obtained in 3–150 keV were fitted well with a combination of a power-law/cut-off power-law, a multicolor-disk blackbody, a smeared edge and a gaussian emission line or a combination of a bulk-motion Comptonization, a high energy cutoff or not and a smeared edge component, i.e. MODEL 1 and MODEL 2.

As can be seen from the spectral fitting results with the phenomenological model of MODEL 1 and the physical model of MODEL 2, the total flux decays by a factor of ~ 3 as it evolves from the hard state into the soft state. This challenges the idea of Esin et al. (1997) that the state transitions of a source are driven by (variations in) the mass accretion rate (\dot{m}). From the results of our physical model fitting with the BMC component, we obtain that the area of the Compton cloud decreases by a factor of ~ 23 during the transition from hard-to-soft, indicating the size of the Comptonizing region to be the second driving factor and further confirming the Homan et al. (2001) results. Recent observations (Rutledge et al. 1999; Homan et al. 2001; Wilson & Done 2001; Revnivtsev et al. 2000; Trudolyubov et al. 2001; Maccarone & Coppi 2003) have also suggested that in addition to \dot{m} there is another parameter responsible for the state of a system. Homan et al. (2001) argued that two independent parameters are needed to describe the states. The second parameter could be the size of the Comptonizing region confirmed by Miller et al. (2004), which is perhaps the compactness of the corona (Homan et al. 2001, 2005). The second parameter may be the disk mass (Yu et al. 2004), the illumination (Dubus et al. 1999), the second photon source in the corona (Kalemci et al. 2006), e.g., synchrotron self compton radiation caused by synchrotron radiation in the corona (Markoff & Nowak 2004), or the magnetic reversals (Livio et al. 2003; Igumenshchev et al. 2003), etc. The factors causing the state and the state transitions are still being argued, and theoretical and observation studies are needed to confirm these factors. If the outer radius of the Comptonizing corona is the inner radius of the optically thick accretion disk, in the case of a Kerr black hole the inner disk radius will be $\sim 1.25R_g$ in the soft state and $\sim 6R_g$ in the hard state. The inner disk radius is $\sim 6R_g$ in the case of the Schwarzschild black hole in the soft state and $\sim 27R_g$ in the hard state. These indicate that the disk is truncated with $\sim 10\text{--}20R_g$ inferred from the derived line width (Done & Gierliński 2006).

If the base of the jet is the corona (Narayan 2005) which carried off part of the accretion material, it will cause a decrease in the total X-ray flux and a shrinkage of the vertical scale of the corona which appears as the decrease of the Comptonizing corona. During the transition from the hard state to the soft state, the frequency typically increases (Rossi et al. 2004), and the power-law photon index is relatively constant. The 250 Hz high-frequency quasi-periodic oscillations (HFQPOs) which appear at 53–139 Hz in the hard state first observed by Homan et al. (2003); the low-frequency quasi-periodic oscillations (LFQPOs) also increase (Montanari et al. 2009). If the QPO frequency is directly related to the transition radius between the cold disk and the hot inner flow (Titarchuk et al. 1999; Psaltis & Norman 2000), then the behavior of the QPOs will also be consistent with a decreasing size scale in the accretion flow when the source changes its state from the hard state to the soft state. Thus, based on the total flux in the 2–100 keV energy range, the jet emission and the timing analysis during the state transition, we suggest a possible geometry and evolution of a (jet+corona+disk) system proposed by Kalemci et al. (2003) based on enhanced lags and a peak frequency shift during the transition, although the geometry of the accretion system in each state and the triggering mechanism for the state transitions are not well understood (Nowak et al. 2002).

Acknowledgements This research has made use of data obtained from the High Energy Astrophysics Science Archive Research Center (HEASARC) provided by NASA's Goddard Space Flight Center. The authors would like to express their hearty thanks to all the members of the RXTE Science Working Group. This work was partially supported by the Grant-in-Aid for Scientific Research on Priority Areas (Grant No. 14079101). We acknowledge financial supports from the National Natural Science Foundation of China (Grant No. 10778702), the National Basic Research Program of China (973 Program, Grant No. 2009CB824800), and the Policy Research Program of Chinese Academy of Sciences (KJ CX2-YWT24).

References

- Anders, E., & Grevesse, N. 1989, *Geochim. Cosmochim. Acta*, 53, 197
- Arnaud, K. A. 1996, in *ASPC Series 101, Astronomical Data Analysis Software and Systems V*, eds. G. H. Jacoby, & J. Barnes, 17
- Belloni, T., Homan, J., Casella, P., et al. 2005, *A&A*, 440, 207
- Belloni, T., Parolin, I., Del Santo, M., et al. 2006, *MNRAS*, 367, 1113
- Blandford, R. D., & Begelman, M. C. 1999, *MNRAS*, 303, L1
- Blandford, R. D., & Payne, D. G. 1981, *MNRAS*, 194, 1041
- Borozdin, K., Revnitsev, M., Trudolyubov, S., Shrader, C., Titarchuk, L. 1999, *ApJ*, 517, 367
- Bradshaw, C. F., Titarchuk, L., & Kuznetsov, S. 2007, *ApJ*, 663, 1225
- Bradt, H., Levine, A., Remillard, R., & Smith, D. A. 2001, *X-ray Astronomy: Stellar Endpoints, AGN, and the Diffuse X-ray Background*, 599, 35
- Bradt, H., & Remillard, R. A. 2001, in *ASPC Series 234, X-ray Astronomy 2000*, eds. R. Giacconi, S. Serio, & L. Stella, 627
- Brocksopp, C., Bandyopadhyay, R. M., & Fender, R. P. 2004, *New Astron.*, 9, 249
- Cadotte Bel, M., Sizun, P., Goldwurm, A., et al. 2006, *A&A*, 446, 591
- Castro-Tirado, A. J., Kilmartin, P., Gilmore, A., et al. 2001, *IAU Circ.*, 7707, 3
- Chen, W., Shrader, C. R., & Livio, M. 1997, *ApJ*, 491, 312
- Chen, Y. P., Zhang, S., Torres, D. F., et al. 2010, *A&A*, 522, A99
- Colpi, M. 1988, *ApJ*, 326, 223
- Coppi, P. 2004, in *AIPC Series 714, X-ray Timing 2003: Rossi and Beyond*, eds. P. Kaaret, F. K. Lamb, & J. H. Swank (Woodbury: AIP), 79
- Coppi, P. S. 1992, *MNRAS*, 258, 657
- Coppi, P. S. 1999, in *ASPC Series 161, High Energy Processes in Accreting Black Holes*, eds. J. Poutanen, & R. Svensson (San Francisco, CA: ASP), 375
- Corbel, S., Fender, R. P., Tomsick, J. A., Tzioumis, A. K., & Tingay, S. 2004, *ApJ*, 617, 1272
- Czerny, B., Różańska, A., Janiuk, A., & Życki, P. T. 2000, *New Astron. Rev.*, 44, 439
- Done, C., & Gierliński, M. 2006, *MNRAS*, 367, 659
- Done, C., Gierliński, M., & Kubota, A. 2007, *A&A Rev.*, 15, 1
- Dove, J. B., Wilms, J., & Begelman, M. C. 1997, *ApJ*, 487, 747
- Dubus, G., Lasota, J.-P., Hameury, J.-M., & Charles, P. 1999, *MNRAS*, 303, 139
- Esin, A. A., McClintock, J. E., & Narayan, R. 1997, *ApJ*, 489, 865
- Fender, R. P. 2001, *MNRAS*, 322, 31
- Ferreira, J., Petrucci, P.-O., Henri, G., Saugé, L., & Pelletier, G. 2006, *A&A*, 447, 813
- Fragile, P. C., & Meier, D. L. 2009, *ApJ*, 693, 771
- Frontera, F., Palazzi, E., Zdziarski, A. A., et al. 2001a, *ApJ*, 546, 1027
- Frontera, F., Zdziarski, A. A., Amati, L., et al. 2001b, *ApJ*, 561, 1006
- Galeev, A. A., Rosner, R., & Vaiana, G. S. 1979, *ApJ*, 229, 318

- Gallo, E., Migliari, S., Markoff, S., et al. 2007, *ApJ*, 670, 600
- Georganopoulos, M., Aharonian, F. A., & Kirk, J. G. 2002, *A&A*, 388, L25
- Gierliński, M., & Newton, J. 2006, *MNRAS*, 370, 837
- Gierlinski, M., Zdziarski, A. A., Done, C., et al. 1997, *MNRAS*, 288, 958
- Gierliński, M., Zdziarski, A. A., Poutanen, J., et al. 1999, *MNRAS*, 309, 496
- Giles, A. B. 1994, in *American Astronomical Society Meeting Abstracts*, *Bulletin of the American Astronomical Society*, 26, 1370
- Groot, P., Tingay, S., Udalski, A., & Miller, J. 2001, *IAU Circ.*, 7708, 4
- Grove, J. E., Johnson, W. N., Kroeger, R. A., et al. 1998, *ApJ*, 500, 899
- Gruber, D. E., Blanco, P. R., Heindl, W. A., et al. 1996, *A&AS*, 120, C641
- Hink, P., Pelling, M., & Rothschild, R. 1992, in *Society of Photo-Optical Instrumentation Engineers (SPIE) Conference Series 1743*, ed. O. H. W. Siegmund, 140
- Homan, J., & Belloni, T. 2005, *Ap&SS*, 300, 107
- Homan, J., Buxton, M., Markoff, S., et al. 2005, *ApJ*, 624, 295
- Homan, J., Klein-Wolt, M., Rossi, S., et al. 2003, *ApJ*, 586, 1262
- Homan, J., Wijnands, R., van der Klis, M., et al. 2001, *ApJS*, 132, 377
- Hua, X.-M., & Titarchuk, L. 1995, *ApJ*, 449, 188
- Ibragimov, A., Poutanen, J., Gilfanov, M., Zdziarski, A. A., & Shrader, C. R. 2005, *MNRAS*, 362, 1435
- Ichimaru, S. 1977, *ApJ*, 214, 840
- Igumenshchev, I. V., & Abramowicz, M. A. 1999, *MNRAS*, 303, 309
- Igumenshchev, I. V., & Abramowicz, M. A. 2000, *ApJS*, 130, 463
- Igumenshchev, I. V., Narayan, R., & Abramowicz, M. A. 2003, *ApJ*, 592, 1042
- Jahoda, K., Black, K., Deines-Jones, P., Hill, J. E., & Swank, J. H. 2008, in *AAS/High Energy Astrophysics Division*, 10, #28.15
- Jahoda, K., Markwardt, C. B., Radeva, Y., et al. 2006, *ApJS*, 163, 401
- Jahoda, K., Swank, J. H., Giles, A. B., et al. 1996, in *Society of Photo-Optical Instrumentation Engineers (SPIE) Conference Series 2808*, eds. O. H. Siegmund, & M. A. Gummin, 59
- Jones, F. C. 1968, *Physical Review*, 167, 1159
- Kalemci, E., Tomsick, J. A., Rothschild, R. E., et al. 2003, *ApJ*, 586, 419
- Kalemci, E., Tomsick, J. A., Rothschild, R. E., et al. 2006, *ApJ*, 639, 340
- Kubota, A., Ebisawa, K., Makishima, K., & Nakazawa, K. 2005, *ApJ*, 631, 1062
- Kubota, A., & Makishima, K. 2004, *ApJ*, 601, 428
- Lamb, P., & Sanford, P. W. 1979, *MNRAS*, 188, 555
- Lasota, J.-P. 2001, *New Astron. Rev.*, 45, 449
- Lasota, J.-P., Narayan, R., & Yi, I. 1996, *A&A*, 314, 813
- Laurent, P., & Titarchuk, L. 1999, *ApJ*, 511, 289
- Levine, A. M., Bradt, H., Cui, W., et al. 1996, *ApJ*, 469, L33
- Lightman, A. P., & White, T. R. 1988, *ApJ*, 335, 57
- Livio, M., Pringle, J. E., & King, A. R. 2003, *ApJ*, 593, 184
- Maccarone, T. J., & Coppi, P. S. 2003, *MNRAS*, 338, 189
- Magdziarz, P., & Zdziarski, A. A. 1995, *MNRAS*, 273, 837
- Maitra, D., Markoff, S., Brocksopp, C., et al. 2009, *MNRAS*, 398, 1638
- Makishima, K., Maejima, Y., Mitsuda, K., et al. 1986, *ApJ*, 308, 635
- Malzac, J. 2007, *Mem. Soc. Astron. Italiana*, 78, 382
- Malzac, J., & Belmont, R. 2009, *MNRAS*, 392, 570
- Malzac, J., Petrucci, P. O., Jourdain, E., et al. 2006, *A&A*, 448, 1125
- Markoff, S., Nowak, M., Corbel, S., Fender, R., & Falcke, H. 2003, *A&A*, 397, 645
- Markoff, S., & Nowak, M. A. 2004, *ApJ*, 609, 972

- Markoff, S., Nowak, M. A., & Wilms, J. 2005, *ApJ*, 635, 1203
- Markwardt, C., Swank, J., & Smith, E. 2001, *IAU Circ.*, 7707, 2
- McClintock, J. E., & Remillard, R. A. 2006, in *Compact Stellar X-ray Sources*, eds. W. Lewin, & M. van der Klis (Cambridge: Cambridge Univ. Press), 157
- McConnell, M. L., Ryan, J. M., Collmar, W., et al. 2000, *ApJ*, 543, 928
- McConnell, M. L., Zdziarski, A. A., Bennett, K., et al. 2002, *ApJ*, 572, 984
- Meier, D. L. 2005, *Ap&SS*, 300, 55
- Merloni, A., & Fabian, A. C. 2002, *MNRAS*, 332, 165
- Migliari, S., Tomsick, J. A., Markoff, S., et al. 2007, *ApJ*, 670, 610
- Miller, J. M., Fabian, A. C., Wijnands, R., et al. 2002, *ApJ*, 570, L69
- Miller, J. M., Raymond, J., Fabian, A. C., et al. 2004, *ApJ*, 601, 450
- Miniutti, G., Fabian, A. C., & Miller, J. M. 2004, *MNRAS*, 351, 466
- Mitsuda, K., Inoue, H., Koyama, K., et al. 1984, *PASJ*, 36, 741
- Montanari, E., Titarchuk, L., & Frontera, F. 2009, *ApJ*, 692, 1597
- Narayan, R. 2005, *Ap&SS*, 300, 177
- Narayan, R., Igumenshchev, I. V., & Abramowicz, M. A. 2000, *ApJ*, 539, 798
- Nishimura, J., Mitsuda, K., & Itoh, M. 1986, *PASJ*, 38, 819
- Nowak, M. A., Wilms, J., & Dove, J. B. 2002, *MNRAS*, 332, 856
- Nowak, M. A., Wilms, J., Heinz, S., et al. 2005, *ApJ*, 626, 1006
- Orosz, J. A., McClintock, J. E., Remillard, R. A., & Corbel, S. 2004, *ApJ*, 616, 376
- Poutanen, J., & Coppi, P. S. 1998, *Physica Scripta Volume T*, 77, 57
- Poutanen, J., & Coppi, P. S. 1998, *Physica Scripta Volume T*, 77, 57
- Poutanen, J., Krolik, J. H., & Ryde, F. 1997, *MNRAS*, 292, L21
- Poutanen, J., & Svensson, R. 1996, *ApJ*, 470, 249
- Pringle, J. E. 1981, *ARA&A*, 19, 137
- Psaltis, D., & Norman, C. 2000, *ArXiv: astro-ph/0001391*
- Quataert, E., & Gruzinov, A. 2000, *ApJ*, 539, 809
- Remillard, R. 2001, *IAU Circ.*, 7707, 1
- Remillard, R. A. 2005, in *22nd Texas Symposium on Relativistic Astrophysics*, eds. P. Chen, E. Bloom, G. Madejski, & V. Patrosian, 79
- Remillard, R. A., & McClintock, J. E. 2006, *ARA&A*, 44, 49
- Revnivtsev, M., & Sunyaev, R. 2001, *IAU Circ.*, 7715, 1
- Revnivtsev, M. G., Trudolyubov, S. P., & Borozdin, K. N. 2000, *MNRAS*, 312, 151
- Rossi, S., Homan, J., Miller, J. M., & Belloni, T. 2005, *MNRAS*, 360, 763
- Rossi, S., Miller, J. M., Homan, J., & Belloni, T. 2004, *Memorie della Societa Astronomica Italiana Supplementi*, 5, 184
- Rothschild, R. E., Blanco, P. R., Gruber, D. E., et al. 1998, *ApJ*, 496, 538
- Rutledge, R. E., Lewin, W. H. G., van der Klis, M., et al. 1999, *ApJS*, 124, 265
- Shakura, N. I., & Sunyaev, R. A. 1973, *A&A*, 24, 337
- Shapiro, S. L., Lightman, A. P., & Eardley, D. M. 1976, *ApJ*, 204, 187
- Shaposhnikov, N., & Titarchuk, L. 2006, *ApJ*, 643, 1098
- Shrader, C. R., & Titarchuk, L. 1999, *ApJ*, 521, L121
- Stone, J. M., Pringle, J. E., & Begelman, M. C. 1999, *MNRAS*, 310, 1002
- Strohmayer, T. 1994, in *American Astronomical Society Meeting Abstracts, Bulletin of the American Astronomical Society*, 26, 1332
- Sunyaev, R. A., & Titarchuk, L. G. 1980, *A&A*, 86, 121
- Sunyaev, R. A., & Truemper, J. 1979, *Nature*, 279, 506

- Tanaka, Y., & Lewin, W. H. G. 1995, in *X-ray Binaries*, eds. W. H. G. Lewin, J. van Paradijs, & E. P. J. van den Heuvel (Cambridge: Cambridge Univ. Press), 126
- Tanaka, Y., & Shibazaki, N. 1996, *ARA&A*, 34, 607
- Titarchuk, L. 1994, *ApJ*, 434, 570
- Titarchuk, L., & Fiorito, R. 2004, *ApJ*, 612, 988
- Titarchuk, L., & Hua, X.-M. 1995, *ApJ*, 452, 226
- Titarchuk, L., & Lyubarskij, Y. 1995, *ApJ*, 450, 876
- Titarchuk, L., Mastichiadis, A., & Kylafis, N. D. 1997, *ApJ*, 487, 834
- Titarchuk, L., Osherovich, V., & Kuznetsov, S. 1999, *ApJ*, 525, L129
- Titarchuk, L., & Seifina, E. 2009, *ApJ*, 706, 1463
- Titarchuk, L., & Shrader, C. R. 2002, *ApJ*, 567, 1057
- Titarchuk, L., & Zannias, T. 1998, *ApJ*, 493, 863
- Tomsick, J. A., Kalemci, E., & Kaaret, P. 2004, *ApJ*, 601, 439
- Tomsick, J. A., Kalemci, E., Kaaret, P., et al. 2008, *ApJ*, 680, 593
- Trudolyubov, S. P., Borozdin, K. N., & Priedhorsky, W. C. 2001, *MNRAS*, 322, 309
- Turolla, R., Zane, S., & Titarchuk, L. 2002, *ApJ*, 576, 349
- Wardziński, G., Zdziarski, A. A., Gierliński, M., et al. 2002, *MNRAS*, 337, 829
- Wayne, L., Heindl, W., & Rothschild, R. 1995, in *American Astronomical Society Meeting Abstracts, Bulletin of the American Astronomical Society*, 27, #121.04
- Wijnands, R., Miller, J. M., & Lewin, W. H. G. 2001, *IAU Circ.*, 7715, 2
- Wilms, J., Nowak, M. A., Pottschmidt, K., Pooley, G. G., & Fritz, S. 2006, *A&A*, 447, 245
- Wilson, C. D., & Done, C. 2001, *MNRAS*, 325, 167
- Yu, W., van der Klis, M., & Fender, R. 2004, *ApJ*, 611, L121
- Yuan, F. 2001, *MNRAS*, 324, 119
- Yuan, F., & Zdziarski, A. A. 2004, *MNRAS*, 354, 953
- Zdziarski, A. A. 2000, in *Highly Energetic Physical Processes and Mechanisms for Emission from Astrophysical Plasmas*, IAU Symposium 195, eds. P. C. H. Martens, S. Tsuruta, & M. A. Weber (New York: Springer), 153
- Zdziarski, A. A., & Gierliński, M. 2004, *Progress of Theoretical Physics Supplement*, 155, 99
- Zdziarski, A. A., Grove, J. E., Poutanen, J., Rao, A. R., & Vadawale, S. V. 2001, *ApJ*, 554, L45
- Zdziarski, A. A., Johnson, W. N., & Magdziarz, P. 1996, *MNRAS*, 283, 193
- Zdziarski, A. A., Lubiński, P., Gilfanov, M., & Revnivtsev, M. 2003, *MNRAS*, 342, 355
- Zdziarski, A. A., Poutanen, J., Paciesas, W. S., & Wen, L. 2002, *ApJ*, 578, 357
- Zhang, G.-B., Qu, J.-L., Zhang, S., et al. 2007, *ApJ*, 659, 1511
- Zhang, W., Giles, A. B., Jahoda, K., et al. 1993, in *Society of Photo-Optical Instrumentation Engineers (SPIE) Conference Series* 2006, ed. O. H. Siegmund, 324
- Zimmerman, E. R., Narayan, R., McClintock, J. E., & Miller, J. M. 2005, *ApJ*, 618, 832